Radiation Physics and Chemistry 162 (2019) 199–207

Contents lists available at ScienceDirect

Radiation Physics and Chemistry

journal homepage: www.elsevier.com/locate/radphyschem

Design and construction of a variable resolution cone-beam small animal mini-CT prototype for in vivo studies

Vahid Lohrabian[a], Alireza Kamali-Asl[a], Hossein Arabi[b], Farugh Mamashi[a], Hamid Reza Hemmati[a], Habib Zaidi[b,c,d,e,*]

[a] Department of Medical Radiation Engineering, Shahid Beheshti University, GC, Tehran, Iran
[b] Division of Nuclear Medicine and Molecular Imaging, Geneva University Hospital, CH-1211 Geneva, Switzerland
[c] Geneva University Neurocenter, Geneva University, 1205 Geneva, Switzerland
[d] Department of Nuclear Medicine and Molecular Imaging, University of Groningen, University Medical Center Groningen, 9700 RB Groningen, Netherlands
[e] Department of Nuclear Medicine, University of Southern Denmark, 500 Odense, Denmark

ARTICLE INFO

Keywords:
X-rays
Analysis
Design
Experiment
Evaluation
Measurement
Mini-CT scanner
Small-animal imaging
Flat panel detector
Spatial resolution

ABSTRACT

We present the conceptual design and construction of a mini x-ray computed tomography (mini-CT) scanner designed and built for in vivo small-animal imaging. The imaging system includes an x-ray tube with 0.5 mm focal spot size and a flat panel detector that provides an active area of 41 × 41 cm^2 with 200 μm × 200 μm pixel size. The scanner, designed based on the rotating sample idea, features variable imaging magnification and field-of-view (FOV). To this end, the detector and x-ray tube are mounted on linear motion systems, such that the object to detector or object to x-ray source distance can be easily changed. The variable magnification enables to acquire images at different spatial resolution depending on the size of the object being imaged. This design provides a trade-off between the scanner's FOV and imaging spatial resolution in which small objects are imaged at relatively high spatial resolution as smaller FOVs are required. Conversely, larger objects can also be imaged as the scanner's FOV is adjustable at the expense of spatial resolution degradation. The scanner's FOV varies from 43 cm down to 9 cm (in diameter) with a spatial resolution improving from 3.9 cycle/mm up to 14.4 cycle/mm, respectively. This mini-CT scanner is a self-standing versatile imager suitable for various preclinical imaging applications.

1. Introduction

X-ray based imaging devices, such as mini/micro computed tomography (CT) scanners, enable the non-destructive visualization of internal structures and have gained considerable importance in a number of applications, including material, geology and medical sciences. Micro- and mini-CT scanners play a pivotal role in biomedical and preclinical research (Bushberg and Boone, 2011) owing to their ability to achieve imaging with high spatial resolution, thus enabling to provide detailed anatomical information (Hu et al., 2011). These devices were broadly used to study vessels, tumors, soft tissues such as lung parenchyma, bony structures, density in osteoporosis, osteoarthritis, microvasculature anatomy and in other fields, such as drug discovery (Badea et al., 2008; Bartling et al., 2007; De Clerck et al., 2004; Paulus et al., 2000). Depending on the application and the target organ, the scanning protocol specifications differ in terms of tube voltage, current, exposure time and number of projections to achieve the desired image contrast (Bretin et al., 2013).

Among the attractive underlying characteristics of mini/micro CT scanner is their capability of providing images with high spatial resolution compared to clinical CT scanners. Although the latter are able to image objects down to a few centimeters in diameter (rats or mice), the spatial resolution would not improve as the object size decreases. Clinical CT scanners are primarily designed for whole-body imaging providing a field-of-view (FOV) in the range of 40–50 cm. Appropriate imaging of anatomical structures hundred times smaller than those of humans requires a CT scanner with enhanced spatial resolution even though a large FOV (similar to clinical CT scanners) is not a necessity. Since the detector resolution is primarily a function of detector element size, the need for high resolution preclinical CT scanners dedicated for small-animal imaging requires detectors with smaller element size (Paulus et al., 2000). However, smaller detector elements lead to increased radiation dose to acquire images with acceptable quality and signal-to-noise ratio (SNR). The lower image quality or SNR associated

* Corresponding author at: Division of Nuclear Medicine and Molecular Imaging, Geneva University Hospital, CH-1211 Geneva, Switzerland.
E-mail address: habib.zaidi@hcuge.ch (H. Zaidi).

https://doi.org/10.1016/j.radphyschem.2018.10.019
Received 17 May 2018; Received in revised form 19 October 2018; Accepted 22 October 2018
Available online 25 October 2018
0969-806X/

Table 1
Key characteristics of micro-, mini- and clinical-scale CT scanners.

	Micro-CT	Mini-CT	Clinical CT
Application	Tissue samples, insects, mice, rats	Mice, rats, rabbits, primates, mini-pigs	Up to humans
Spatial resolution (isotropic)	5 μm (single limbs) – 100 μm (whole animals)	100–450 μm	> 450 μm (z-axis > 600 μm)
Transaxial FOV	1–5 cm	5–20 cm	> 20 cm
Time to acquire a "standard" volume (e.g., whole animal)	Seconds to hours (CT scanners with single slice acquisition)	Subsecond (0.5 s) to a few seconds	Few seconds (with rotation times down to 0.33 s)
Radiation dose	> 1 Gy can be reached	~10–500 mGy	< 50 mGy
Design	Bench-top, rotating sample (with variable geometry, resolution, scan FOV, etc.) or rotating gantry	Rotating specimen or rotating gantry (fixed geometry)	Rotating gantry (fixed geometry)

with smaller detector element area is compensated by increasing the tube current and/or the exposure time per projection (compared to conventional CT scanners) (Ford et al., 2003). Therefore, there is no single scanner design capable of optimizing all the fundamental imaging parameters, including spatial resolution, radiation dose, acquisition time, … etc. Instead, various scanner designs suitable for different requirements and applications were proposed as summarized in Table 1. Clinical CT scanners provide large FOV but only moderate spatial resolution. Conversely, small-animal CT scanners are suitable for imaging small objects owing to the enhanced spatial resolution at the expense of a smaller FOV (typically a few centimeters).

The interest in in vivo small laboratory animal imaging raised as a result of the success of tracking molecular mechanisms associated with human diseases in living small-animal models. With the advent of small-animal imaging, cross-sectional study approaches (e.g., where cohorts of animals are killed at each time point and histology is examined) were replaced by in vivo study designs allowing repeated examination of the same animals. There is no unique definition for mini-CT and micro-CT and often all CT scanners providing significantly higher spatial resolution than conventional clinical scanners are called micro-CT. Considering the constraints associated with different designs of CT scanners, the term mini-CT is used to describe CT scanners with a resolution ranging from 100 μm to 500 μm whereas micro-CT refers to scanners having a resolution below 100 μm. Overall, they are divided into two configuration-wise categories: rotating sample- and rotating gantry-based designs. Scanners referred to as rotating samples feature a fixed x-ray source and detector facing each other and a rotating table placed between the source and the detector (Bartling et al., 2007). The sample is placed on a table that rotates around the center of the FOV (Paulus et al., 2000; Zhu et al., 2009a, 2009b). The second type is the rotating gantry in which the detector and x-ray source face each other in a circle with a fixed radius from the center of rotation. They are mounted on a gantry rotating around the sample table (Bartling et al., 2007). Each of these settings has its own advantages and drawbacks. For the rotating gantry type, animal setup and positioning is easier and the gantry can rotate faster at the cost of complex mechanical design and control system (Badea et al., 2004; Vaquero et al., 2008; Zainon et al., 2010).

Conversely, relatively simple mechanical design, control and lower manufacturing cost are the advantages of the sample rotating type (Casali et al., 2003; Lin and Miller, 1996).

Regardless of the design configuration, most preclinical CT imagers provide fixed spatial resolution and FOV whereas the size of objects under study may vary (Melnyk and DiBianca, 2007). Given a small object down to 1 cm in diameter, a CT scanner with high spatial resolution is highly desirable to depict tiny internal structures. In addition, the scanner's FOV is not a matter of concern owing to the small size of the object. Conversely, for a larger object, up to 30 cm in diameter, a large FOV scanner that accommodates the object is needed in the first place. This is usually achieved at the expense of a lower spatial resolution, which remains acceptable owing to the larger internal structures. A versatile scanner offering these two possibilities would be very practical as it covers a wide range of applications. To this end, we have designed and built a mini-CT scanner based on the sample rotating configuration which provides variable spatial resolution and FOV. In the sample rotating configuration, the radiation source and detector are commonly set at fixed distances, thus limiting the scanner's resolution capabilities (Hutchinson et al., 2017). However, an advantage of the sample rotating configuration is that it allows easy adjustment of the object to detector (or to source) distance to achieve variable FOV and spatial resolution through modifying the scanner magnification (Hutchinson et al., 2017). The detector and x-ray source are mounted on two independent motorized linear motion systems to allow variable source to table and detector to table distances (sample table is fixed). Through varying the object to table distance (or source to table distance), different magnifications can be achieved, which determines the spatial resolution. Higher magnification leads to higher imaging spatial resolution at the cost of reduction in the scanner's FOV. This configuration enables to adjust the spatial resolution and FOV according to object size. As a result, small objects can be imaged at a relatively higher spatial resolution and smaller FOV while large objects can be imaged at a relatively larger FOV and consequently lower spatial resolution.

Similar to this work, a versatile CT scanner was previously proposed based on a variable resolution x-ray (VRX) detector (Melnyk and DiBianca, 2007). In this VRX CT scanner, a one-dimensional discrete detector is placed at an acute angle with respect to the x-ray tube and the incident beam. Through detector angulation, the width and sampling distance of physical (or virtual) detector elements appear to be smaller due to the projective compression principle. Therefore, the spatial resolution can be improved at least a few orders of magnitude. The VRX CT scanner offers a spatial resolution varying from 1.4 cycles/mm to 43 cycles/mm as the FOV decreases from 32 cm to 1 cm. The proposed small-animal scanner differs from the VRX CT scanner as a flat-panel detector is employed in this study (as opposed to the VRX CT scanner equipped with a one-dimensional detector array), which offers a large axial coverage suitable for dynamic imaging. The angulation of the detector in the VRX CT scanner not only adds to mechanical complexity of the scanner but also improves the spatial resolution in the transaxial plane only, while the axial resolution remains unchanged. However, the spatial resolution varies isotropically in the proposed design as the system magnification changes equally in both axial and transaxial directions.

2. Materials and methods

2.1. System description

The mini-CT scanner was designed based on the sample rotating idea having the capability of achieving variable magnification. The main aim of this work is to provide variable FOV to accommodate objects with different sizes while the scanner's spatial resolution varies according to the object size. The FOV and spatial resolution in this design change conjointly as a function of scanner magnification. To

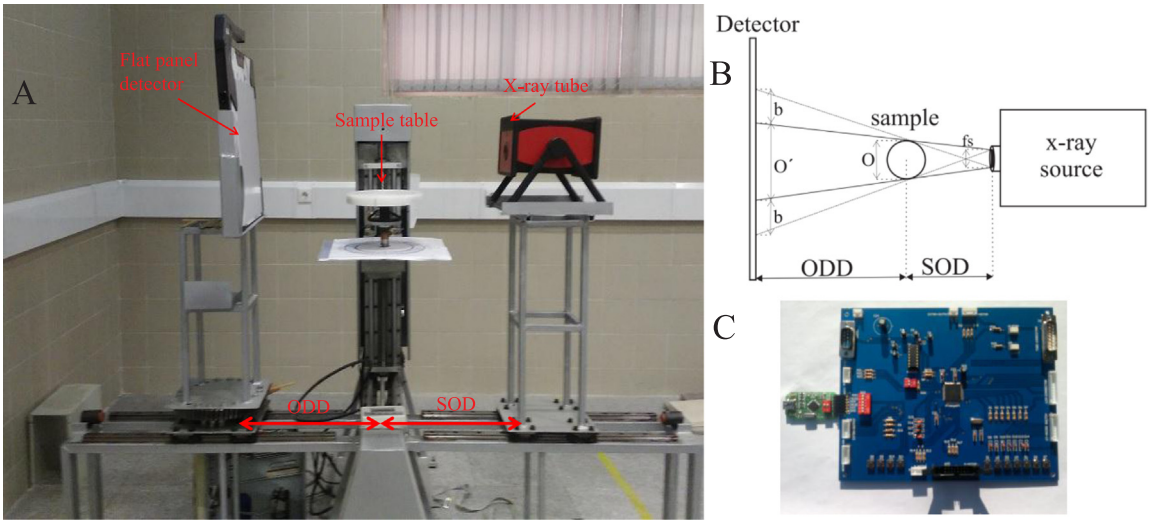

Fig. 1. (A) Cone-beam animal mini-CT prototype with fixed gantry design (SOD refers to source to object distance whereas ODD refers to object to detector distance). (B) Schematic diagram of the mini-CT scanner geometry. (C) Electronic board of the main control system.

achieve variable magnification, the detector and x-ray tube are mounted on two translational motion systems, such that the source to object distance (SOD) and object to detector distance (ODD) can be easily adjusted. The detector and source translational motion systems consist of 2 linear ball screw components with 12.5 μm motion precision and a rotating system with 0.3° angular precision per step. As depicted in Fig. 1A, the sample bed is mounted on a fixed arm capable of spinning the samples for tomographic imaging. Three stepper motors support translational and rotational movements controlled by an electronic board interfacing the scanner and the computer.

2.1.1. X-ray tube

A dedicated x-ray source, depending on the specific application of the small-animal CT scanner, should have one or all of these three important properties: a small focal spot size to achieve high spatial resolution, capability of emitting high photon flux compared to those used in conventional CT scanners, and x-ray energies selectable over a desirable range to generate appropriate image contrast (Bartling et al., 2007). A portable cone-beam x-ray tube (Medex instrument, model GemX-160) with a focal spot of 0.5 × 0.7 mm^2 (500 μm nominal focal spot) and power supply 28–35 Vdc LiPo battery was employed. The x-ray tube is capable of target voltages ranging from 20 to 160 kVp (typically 30–140 kVp), with a maximum beam current of 2 mA (typically 0.1–2 mA). The x-ray source is a mini-focus source with fixed tungsten anode of 0.8 × 0.8 mm^2 area. The source emits a conic x-ray beam with a coverage of 1.23 sr (35.3°) and has an inherent filtration of 150 μm of beryllium. The tube can be easily regulated by a remote controller attached to a computer. In this study, only the intrinsic Berillium filter was used for beam filtering. We designed a supplementary electronic board that controls this x-ray tube by which the x-ray exposure time, kV_p and anode current can be adjusted and monitored by a LCD connected to the designed electronic board.

2.1.2. Flat-panel detector

The detector element size plays a critical role in determining the spatial resolution of the mini-CT scanner (Song et al., 2001). Flat-panel detectors featuring a large active area enable CT scanners to cover a large volume per rotation which would result in a faster scan time. Moreover, a higher magnification and consequently higher spatial resolution can be achieved. Wide axial coverage of flat-panel detectors enables whole-body imaging of animals in one bed position. *a*-Si flat-panel detectors provide many advantages, such as large-area detection, thin structure, no geometrical distortions, highly efficient collection of emitted light and veiling glares (Seibert, 2006). The detector used in this work is a Si/GadOx flat-panel detector (DeReO WA1) produced by X-RIS (ANS, Belgium). The active area of the detector is 41 × 41 cm^2 (2048 × 2048 pixels) with a pixel size of 200 μm. The detector is fixed to a mechanical support mounted on the translational motion structure to create an angle of 90° between the center of the detector and the incident x-ray beam.

2.1.3. Scanner geometry

Regardless of the type of x-ray source and detector, the CT scanner geometry can be classified into two categories: the so-called "short" scanner geometry where the SOD is small compared to the ODD and the "long" scanner geometry where the SOD is equal to the ODD (ODD and SOD are indicated in Fig. 1A and B) (Bartling et al., 2007). The SOD and ODD play a key role in x-ray imaging as they determine the magnification factor and consequently affect the spatial resolution and FOV of the scanner. The image will be projected onto the detector by the magnification factor (*M*) determined solely by ODD and SOD (Eq. (1)):

$$M = 1 + \frac{ODD}{SOD} \tag{1}$$

Three factors influence the resolution of the final image: x-ray source focal spot size (*fs*), the detector array resolution and subject position with respect to the source and detector (which determines imaging magnification) (Paulus et al., 2000). A non-ideal x-ray tube with finite focal spot size causes penumbral blurring that limits the spatial resolution in the projection plane. The relationship between the x-ray tube focal spot size (*fs*) and the resulting spatial resolution (penumbral blurring) (*b*) is governed by Eq. (2) (Badea et al., 2008). In Fig. 1B, the object is presented by a circle whose diameter (i.e., the maximum size of the object) determines the scanner's FOV.

$$b = \frac{ODD}{SOD} fs \tag{2}$$

As shown in Eqs. (1) and (2) and Fig. 1B, when scanning is performed with the object closer to the source, the magnification factor increases and consequently the detector resolution will improve. However, the FOV of the system decreases and penumbral blurring also tends to increase (Badea et al., 2008; Bartling et al., 2007; Paulus et al., 2000).

In this work, the flat-panel detector and the cone-beam tube are placed on two linear movement systems facing each other so that their distance from the center of the sample table can be modified. The minimum SOD and maximum ODD in this design are 10 cm and 75 cm,

Table 2
Summary of the main parameters and dimensions of the various components of the scanner, including the x-ray tube and flat-panel detector.

X-ray source	Flat-panel detector	Scanner geometry
Medex instrument (Model GemX-160), focal spot size of 0.5 mm	Si/GadOx flat-panel (DeReO WA1)	"Short" scanner
Tungsten anode	Produced by X-RIS (Ans, Belgium)	Source object fixed distance $D = 10$ cm
High voltage power 20–160 kV_p	Active area: 41 × 41 cm^2 (2048 × 2048 pixels)	Object detector fixed distance = 75 cm
Anode current [0.1–2 mA]	Pixel size of 200 μm	M = 1–7.5

respectively. As such, the magnification factor varies between 1 and 7.5.

2.1.4. Electronic boards

An electronic board was designed for the purpose of controlling and monitoring the motorized movements and x-ray tube parameters. The processor of this board is ATMEGA 64 microcontroller (Atmel, San Jose, CA, USA). The board is connected to the PC by an RS-232 interface and is used to control the three stepper motors that produce the mechanical force for positioning of the source and detector arms as well as table rotation (Fig. 1C). Table 2 presents the major parameters and dimensions of the scanner, including the x-ray tube and flat-panel detector properties.

2.2. Experimental evaluation

The performance characteristics of the developed mini-CT scanner were evaluated in planar and tomographic modes. The variable spatial resolution of the scanner was measured in 2-D or planar imaging mode. The measurements were performed for the different FOVs (each FOV corresponding to a specific magnification) of the scanner. Subsequently, the spatial resolution was reported as a function of the scanner's FOV. The tomographic evaluation of the scanner was performed using a 3-D scan of an anesthetized rat. The lung, heart, and bony structures were segmented to evaluate organs conspicuity in tomographic imaging. In the following, we elaborate on the procedure followed to optimize the x-ray tube voltage, spatial resolution measurements and tomographic imaging of the rat.

2.2.1. Contrast vs. tube voltage

The x-ray tube voltage plays a key role to project the inherent contrast of the object into the image domain and, as such, its optimization is crucial. To this end, we chose to use the Hawkeye quality control (QC) phantom (GE Healthcare, Waukesha, WI, USA) to assess image quality. The phantom consists of a plastic container in the form of a 20 cm diameter cylinder containing water and a set of plastic test inserts. Fig. 2A and B depict a view of the Hawkeye QC phantom together with a schematic plot of the phantom as well as its plastic inserts. The inserts are designed for assessment of the spatial resolution through a range of water/plastic bar patterns which are placed diagonally across the phantom. The bar patterns represent spatial frequencies of 2.0, 2.5, 3.0, 3.5, and 4.0 line pairs/cm. In this experiment, the phantom was filled with pure water and the 3.0 pairs/cm bars were chosen to measure the contrast as a function of tube voltage. The thin plastic inserts create a low contrast (2.5%) against the surrounding water. The contrast between the plastic insert and the surrounding water was measured using Eq. (3). Here In_{bg} indicates the intensity of the background, which in this case is the water content part of the phantom and In_{ob} is the intensity of the object, which is the plastic insert. The x-ray tube voltage was varied from 30 to 100 kVp. The tube voltage generating the maximum contrast was chosen for tomographic imaging and for performing the remaining experiments. Fig. 2C and D show a representative image of the phantom along with the profile depicting the projected contrast between the plastic insert and surrounding water.

$$Ctrs = \frac{|In_{bg} - In_{ob}|}{In_{bg} + In_{ob}} \quad (3)$$

2.2.2. Spatial resolution measurement

The modulation transfer function (MTF) is deemed to be a standard measure of the spatial resolution of imaging systems providing an account of the transfer of sinusoidal inputs through the system. The MTF is an ideal measure for performance evaluation of an imager in terms of spatial resolution. The experimental characterization of detector MTF is usually performed through measurement of the corresponding line spread function (LSF) or edge spread function (ESF) (Khodadad et al., 2011). The LSF and ESF, respectively, are defined as the intensity distribution in the images of perfectly attenuating line and edge objects of unit intensity. The ESF can be easily converted to LSF through performing differentiation on ESF. Similarly, the point spread function (PSF) of a system can be derived by performing a second differentiation. For 2D discrete detectors, the ESF can be measured by imaging a perfectly blocking plate with a sharp edge. Once the system ESF is measured, the corresponding MTF can be computed as (Dobbins et al., 1995; Samei et al., 2006):

$$MTF(f) = c|F\{PSF(x)\}| \quad (4)$$

where F represents the Fourier transform, c is a normalization constant, and x and f are the spatial and frequency coordinates, respectively. Quantification of the system MTF is performed by evaluating the corresponding PSF.

In this experiment, a thick block of lead (2 cm thickness, 10 × 10 cm^2 area) having a neat and sharp edge was used to compute the ESF of the system. Image acquisition was performed at different magnification factors. The magnification of the system was changed as follows: 1.33, 1.47, 1.64, 1.86, 2.14, 2.54, 3.10, 3.99, 5.59, and 6.10. The SOD was fixed at 70 cm for all the aforementioned magnifications and different magnification factors were achieved through displacing the detector which consequently altered the FOV of the system. The corresponding FOV of the system at each magnification is reported in Table 4. A fixed tube voltage of 50 kVp and current of 1700 μA were used for all imaging experiments with an acquisition time of 5 s. These values were obtained from the previous section where the optimal x-tube voltage to achieve the highest image contrast in the phantom study was determined.

Given the 2D projections of the lead block acquired at different magnifications, a cross profile of the obtained images provides the ESF of the system (Fig. 5A). A second differentiation of the ESF function produces the PSF of the scanner, which enables to compute the MTF using Eq. (4). Therefore, at each magnification, the corresponding ESF was derived from the obtained image and the PSF calculated by taking the second differentiation of the ESF. Thereafter, the MTF was computed using the obtained PSF. The spatial frequency corresponding to an MTF of 0.1 was chosen as reference (referred to as cut-off frequency in the literature) to report the spatial resolution of the scanner at each magnification. Moreover, a Gaussian fitting was performed on the PSF obtained at each magnification and its full width at half maximum (FWHM) calculated and reported together with the MTF cut-off frequency. This procedure was repeated for the entire aforementioned magnifications and the spatial resolution reported as a function of the

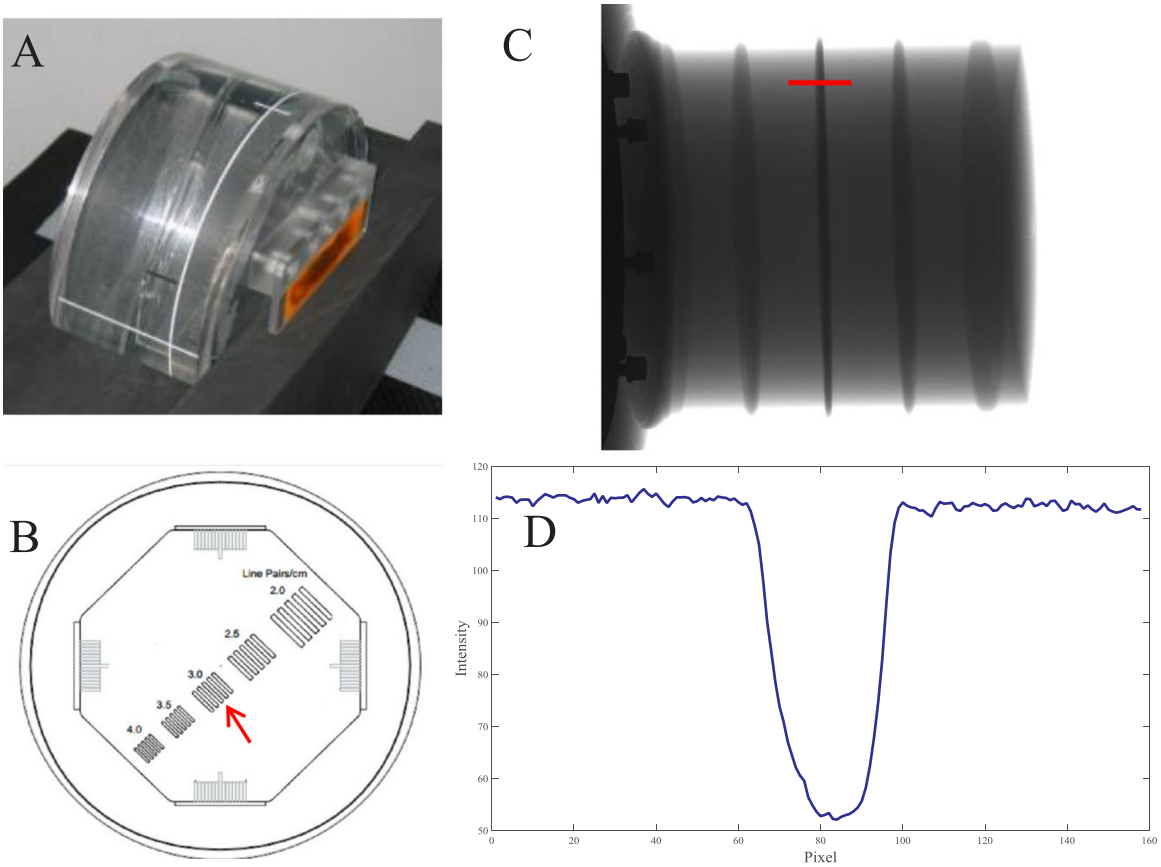

Fig. 2. (A) Hawkeye quality control phantom. (B) The plastic inserts for spatial resolution assessment (3.0 pairs/cm was chosen for contrast measurement). (C) A representative image of the phantom obtained at tube voltage of 50 kVp. (D) Profile of the signal intensity across the plastic insert.

system magnification (or FOV). It should be mentioned that to minimize the impact of noise and local fluctuation of the detector, the ESF of the scanner at each FOV was calculated based on the average of 10 profiles at different locations within the image.

2.2.3. Tomographic imaging

The evaluation in tomographic mode was carried out by 3-D scanning of a normal rat (~317 g weight, 24 cm length including the tail, and ~7 cm diameter). Tomographic imaging was performed with a magnification $M \cong 2.4$. To this end, the gantry geometry was configured with SOD = 26 cm and ODD = 37 cm to achieve the desirable magnification. Fig. 3 shows the scanner geometrical configuration and animal positioning. The animal was fixed in a cylindrical sample holder made of thin sheet of Polymethylmethacrylate with 8 cm diameter and 25 cm length. The animal was anesthetized with 100 mg/kg dose of ketamine hydrochloride to ensure immobilization during the whole scan.

The x-ray tube voltage achieving the highest contrast was previously optimized using the Hawkeye QC phantom. To verify the effectiveness of the optimal tube voltage (50 kV_p) in animal imaging, several 2-D images of the rat were taken by varying the x-ray tube voltage from 30 kV_p to 70 kV_p with 20 ms exposure time per projection (at 1.7 mA). In agreement with the phantom study, the highest image quality in 2-D mode was achieved with a tube voltage of 50 kV_p. The tomographic scan of the rat was performed using 150 projections with 20 ms exposure time per projection over a circular rotation of 180° (step angle of 1.2°). The Feldkamp-David-Kress (FDK) filtered backprojection algorithm was adopted for 3D reconstruction of cone-beam CT data (Feldkamp et al., 1984). This algorithm is a generalization of filtered backprojection in such a way that each voxel in the final image is calculated as a weighted sum of cosine-corrected filtered projections. The modified FDK algorithm, which includes beam hardening correction, was adapted to the specific geometry of our mini-CT scanner.

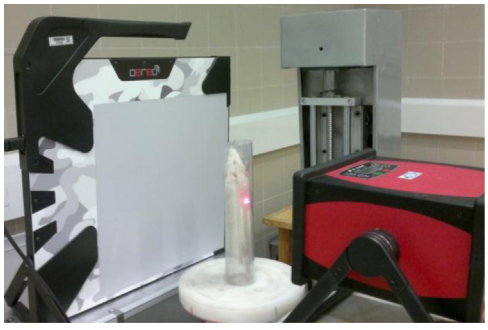

Fig. 3. The rat was fixed in an animal holder placed at SOD = 26 cm and ODD = 37 cm.

After tomographic scanning of the rat, 3D segmentation of organs from the reconstructed image was performed using *Materialise Mimics* image processing software, version 10.01, Leuven Belgium.[1] Axial slices (512 × 512 pixels) were imported into *Mimics*. Image segmentation was performed to extract the heart, lungs and bony structures to assess organs' conspicuity and internal tissues discrimination. To this end, the bony structures in the chest region were extracted by applying an intensity threshold of 100 HU. A region growing algorithm was employed to delineate the heart and lungs through manually placement of the initial seed points. The algorithm scrutinizes neighboring voxels of the initial seed points to determine if the adjacent voxels should be labeled

[1] http://www.materialise.com.

Table 3
Contrast as a function of the x-ray tube voltage obtained using Eq. (3).

Tube voltage (kVp)	Contrast
30	0.27
40	0.32
50	0.36
60	0.32
70	0.28
80	0.23
100	0.20

as lung or heart.

3. Results

Table 3 presents the contrast vs. x-ray tube voltage varying from 30 to 100 kVp measured between the background water and the plastic insert with 2.5% inherent contrast. This range of x-ray voltage is usually suitable to image small-animals, such as rats and mice, to generate appropriate tissue contrast. Evidently, the maximum contrast in planar imaging achieved at the energy of 50 kVp which was chosen for subsequent experiments including the spatial resolution measurement and tomographic imaging. Different x-ray tube voltages were examined in planar imaging of the rat to determine the highest contrast, which occurred at 50 kVp voltage, in agreement with the phantom study. Fig. 4 shows a representative planar image taken from a rat at 50 kVp tube voltage exhibiting proper contrast between the bone, lung and soft tissues.

Table 4 demonstrates this concept where the spatial resolution and scanner's FOV vary jointly as a function of the system magnification.

Fig. 4. A sample of whole-body planar image of the rat with 50 kVp, 1700 μA, 2 ms exposure time and magnification of 2.4.

Table 4
Spatial resolution of the mini-CT scanner in terms of MTF cut-off frequency and FWHM of the PSF measured at different magnifications/FOVs. The scanner provides a variable FOV to enable customizing magnification and spatial resolution.

Magnification	FOV (cm)	FWHM (mm)	MTF (cycle/mm)
1.33	43.58	0.21	3.92
1.47	39.43	0.18	4.33
1.64	35.28	0.16	4.83
1.86	31.13	0.14	5.45
2.14	26.98	0.13	6.30
2.54	22.83	0.11	7.40
3.10	18.68	0.09	9.00
3.99	14.53	0.08	10.76
5.59	10.38	0.06	14.47
6.10	09.05	0.06	14.40

The spatial resolution is reported in Table 4 in terms of MTF cut-off frequency, which corresponds to the frequency (mm/cycle) at which the MTF drops to 0.1. This frequency is assumed to be the highest detectable frequency. As mentioned earlier, both FWHM and MTF were calculated based on the average of 10 profiles at different locations in the detector. Systematic improvements in scanner's spatial resolution were observed as the magnification increases from 1.33 to 6.10 when the scanner's FOV decreases from 43 to 9 cm. The smallest FOV (9 cm) corresponds to a spatial resolution of 14.4 (cycles/mm), good enough for a number of small-animal studies. Fig. 5B shows a representative ESF of the scanner obtained at a magnification of 1.33 and the corresponding PSF (Fig. 5C) calculated by taking the derivative of the ESF. The MTF presented in Fig. 5D depicts the frequency response of the scanner at the highest spatial resolution (corresponding to the largest FOV of 43 cm) where the cut-off frequency is 3.92 (cycles/mm).

Representative views of the tomographic scan of the rat with a magnification of 2.4 are illustrated in Fig. 6. Visual inspection revealed appropriate contrast between bone, lungs and soft-tissue. Since the sampling trajectory from spiral cone-beam scanning does not satisfy Tuy's data sufficiency condition (Tuy, 1983), exact reconstruction is impossible owing to insufficient data (Badea et al., 2008; Holdsworth and Thornton, 2002). Due to the approximate nature of the FDK algorithm, the reconstructed images sometimes suffer from the presence of artifacts, such as low-intensity streaks when the cone angle is large. However, the image quality of the reconstructed images is acceptable if the cone angle is less than about 10° (Holdsworth and Thornton, 2002), except for very unusual cases (Defrise and Clack, 1995). Different filters were implemented including the Shepp & Logan filter, which was chosen for this study due to its better performance. The reconstructed matrix size was 512 × 512 pixels as it satisfies the Nyquist sampling theorem. Since geometric parameters, such as the center of rotation and the off-axis center, impact image quality, proper choice of these parameters was performed.

3D segmentations of the heart, lungs and bone in the chest region are presented in Fig. 7. Although simple segmentation algorithms, such as intensity thresholding for the bone and region growing for the heart and lungs were employed, the organs were properly delineated owing to the strong contrast between the different tissues. Detailed structures and outlines of the organs are visible as the tomographic scan was performed at a magnification of 2.4 corresponding to a spatial resolution of ~7 cycles/mm.

4. Discussion

The main aim of this work was to present the conceptual design of a mini-CT scanner capable of providing jointly variable FOV and spatial resolution to cover a wide range of preclinical applications. Variable spatial resolution was achieved through modifying the magnification of the scanner. To this end, a large detector is required to support a large

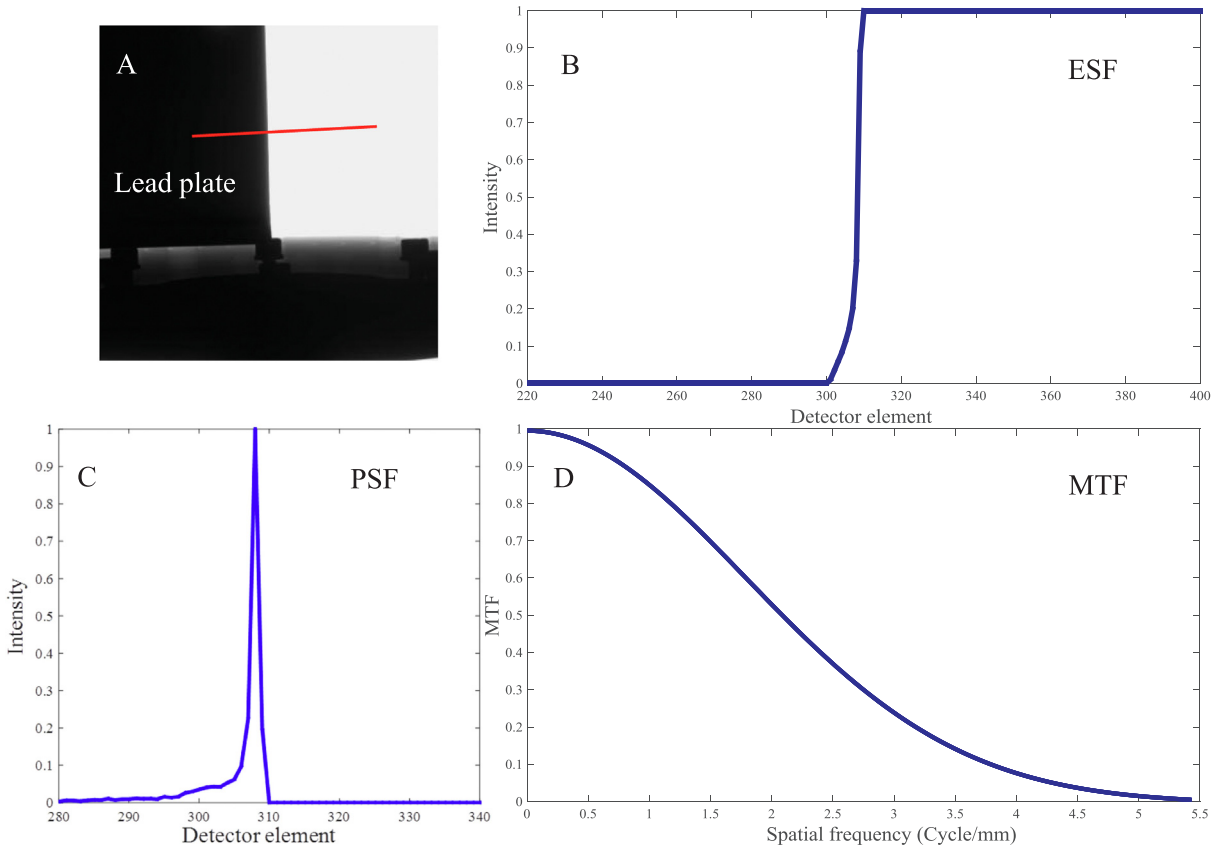

Fig. 5. (A) Representative image of the lead block obtained at 1.33 magnification. (B) The ESF of the scanner corresponding to the red line on image (A). (C) The PSF and (D) MTF of the CT scanner. (For the interpretation of color in this figure, the reader is referred to the web version of this article.)

FOV or high magnification factor. The Si/GadOx flat-panel detector selected for this scanner not only provides a large detection area (41 cm × 41 cm) to support a large FOV, but also very small detector elements (200 μm) that enable achieving high spatial resolution. The large axial coverage allows multi-slice (or cone-beam) imaging, thus enabling to dramatically reduce the scanning time. Moreover, for some applications, such as coronary blood flow, fluoroscopic and angiographic capabilities, large flat-panel detectors are highly recommended (Bartling et al., 2007; Gupta et al., 2008).

A potential application of the developed mini-CT scanner is in vivo dynamic small-animal imaging. However, 4D image acquisition of moving targets becomes very challenging owing to their small size. A limiting factor in this regard is the small size of the focal spot to support a high photons flux. In some dynamic imaging applications, physiologic (respiratory) motion may not be very fast requiring extremely short exposure times. However, cardiac imaging necessitates exposure times in the order of 10 ms to minimize the blurring effect brought by heart motion. To deliver adequate photon flux in such a short exposure time, higher focal spot sizes are required (Badea et al., 2008). Therefore, a number of commercial scanners, equipped with a rotating gantry design, utilize x-ray tubes with large focal spot sizes to circumvent this problem (Bartling et al., 2007; Ross et al., 2006). Diagnostic x-ray tubes were used on these systems with a typical focal spot size of 0.5 or 0.7 mm, similar to our design concept (0.5 mm), to meet the

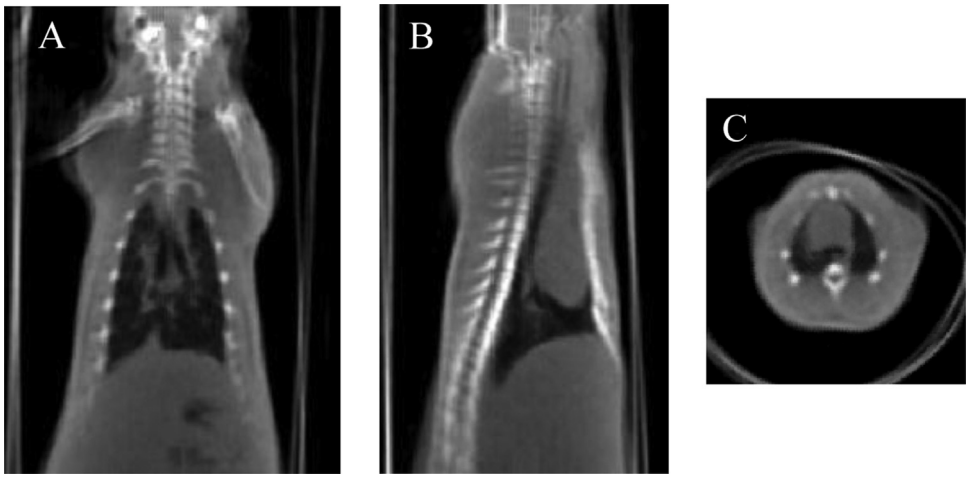

Fig. 6. Representative (A) coronal, (B) sagittal and (C) transverse views of a rat scan reconstructed using the FDK algorithm.

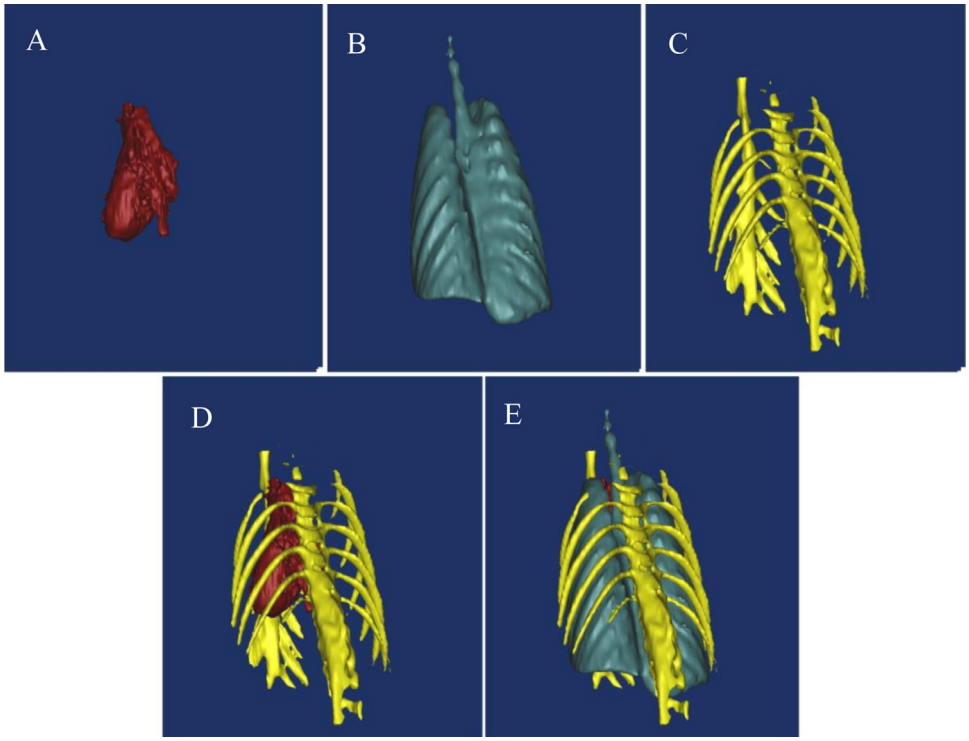

Fig. 7. Representative volumetric organ segmentation from the reconstructed rat image showing: (A) Heart, (B) lung, (C) rib cage, (D) heart inside the rib cage and (E) all organs together.

requirements of the envisaged applications of this scanner. Although the relatively large x-ray focal spot size hampers the spatial resolution, the high photon flux (along with the flat-panel detector) allows very short acquisition time suitable for dynamic studies.

The x-ray tube voltage was determined for a specific application involving medium size rat and static imaging. The optimized voltage based on low intrinsic contrast existing between water and the plastic inserts in the Hawkeye phantom resulted in acceptable lung versus soft-tissue as well as soft-tissue versus bone contrast (Fig. 6). However, for other applications involving larger or smaller animals or dynamic imaging, the x-ray tube voltage should be modified accordingly to achieve acceptable image contrast. The rat tomographic scan presented in Fig. 6 suffers from motion artifacts as slight blurring due to slight trembling of the animal is observed around organ boundaries.

The representative plots of the PSF depicted in Fig. 5 show an asymmetric behavior as the left side of the signal did not fall sharply similar to the right side. This effect was observed almost in all PSF plots and seems to stem from photon scattering and penetration through the edge of the lead plate rather than the detector non-uniform response.

In this mini-CT scanner, the variable spatial resolution solely arises from modification of magnification. It should be noted that the higher magnification tends to only improve the sampling resolution of the detector while having adverse impact on geometric unsharpness (Arabi et al., 2010, 2011). Geometric unsharpness refers to the loss of definition since the x-ray beam does not originate from an infinite point source but rather over an area. The loss of definition (resolution), arising from infinite focal spot limitation, occurs because of penumbra effect, which is a region partially irradiated (imperfect shadow) by x-rays not originating from a point source. Technically, magnification introduces a trade-off between detector sampling resolution and geometric unshaprness (Arabi et al., 2015; Kamali-Asl et al., 2009). Therefore, the spatial resolution is greatly limited by the penumbra effect at high magnification. Considering Table 4, a magnification higher than 5.5 did not improve the spatial resolution of the scanner anymore because of the increased geometric unshaprness. To achieve a higher spatial resolution through increasing the system magnification, the x-ray source with a focal spot size smaller than 0.5 mm is needed to minimize the impact of geometric sharpness. However, a focal spot of 0.5 mm was intentionally exploited in this design to afford the high photon flux required in dynamic imaging. Since dynamic imaging was the main application for this particular scanner, a larger x-ray focal spot was utilized and its adverse impact on spatial resolution compensated through varying the magnification.

In vivo animal CT imaging offers unique information on the time-related changes in internal structures of living mice. However, ionizing radiation might induce side effects on the underlying tissues, an issue that plays a key role in longitudinal studies. Lowering the radiation dose through decreasing the x-ray tube exposure time or photon flux inevitably influences image quality. The absorbed dose to the animal was not directly estimated; however, the scanning parameters used in this study are comparable to typical protocols used in micro-CT imaging of mouse with no significant radiation-induced side effects. A typical CT protocol for mouse scanning with the following parameters: 50 kV, 100 μA, 199 projections and 1 s scan duration per projection, does not lead to noticeable radiation-induced side effects (Laperre et al., 2011). Since the animal CT scan was carried out with much shorter acquisition time per projection (20 ms) and lower number of projections (150), the absorbed dose should be comparable with common protocols.

The aim of this work is to develop a versatile animal scanner capable of supporting a wide range of applications owing to its adjustable FOV and spatial resolution. This is not the first scanner offering these functionalities as the VRX scanner was developed for the same purpose. However, there are major differences between the proposed design and the VRX CT scanner which motivated this contribution. The VRX CT scanner employs two one-dimensional detector arms which rotate around a common pivotal point to provide variable spatial resolution (Melnyk and DiBianca, 2007). A number of drawbacks are associated with this scanner, which are eliminated in the proposed design. Firstly, apart from the mechanical complexity, angulation of the detector with respect to the incident x-ray beam causes significant magnification non-uniformity (and consequently spatial resolution non-uniformity) from one end of the detector to the other. Moreover, due to the non-

perpendicular angle between the incident x-ray beam and the detector, the cross-talk between detector cells increased remarkably which adversely influence the scanner's spatial resolution (Arabi et al., 2011). Since the variable spatial resolution is achieved through modifying the system magnification, no magnification non-uniformity across the detector and no additional inter-cells cross-talk occurs when the scanner's FOV changes. Secondly, the spatial resolution enhancement in the VRX CT scanner only occurs in the transaxial plane while the scanner's axial resolution remains intact. To improve the axial spatial resolution, the VRX detectors should rotate around two axes which further adds to the mechanical complexity of the scanner. This issue is resolved in the proposed CT scanner as the system magnification varies uniformly across the flat-panel detector, which results in isotropic spatial resolution. Third, the VRX CT suffers from long acquisition time due to the use of a single one-dimensional detector; however, multi-slice (or cone-beam) CT scanning can be easily performed on this design owing to the large size of the flat-panel detector.

5. Conclusion

A mini-CT scanner capable of operating as an independent and self-standing imaging device was designed and built. This device features, in addition to very simple design and low manufacturing cost, independent adjustment of the magnification factor to achieve jointly variable spatial resolution and FOV. The spatial resolution of the scanner varies from 3.9 cycles/mm to 14.4 cycles/mm while the FOV decreases from 43 cm to 9 cm, respectively. The mini-CT scanner is equipped with a high flux x-ray tube to support a wide range of applications requiring dynamic scanning. However, the large focal spot size of the tube (0.5 mm) greatly constrains the spatial resolution at high magnifications.

Acknowledgements

This work was supported by the Swiss National Science Foundation, Switzerland, under Grant no. SNSF 320030_176052.

References

Arabi, H., Asl, A.K., Aghamiri, S., 2010. The effect of focal spot size on the spatial resolution of variable resolution X-ray CT scanner. Iran. J. Radiat. Res. 8, 37–43.

Arabi, H., Asl, A.R.K., Ay, M.R., Zaidi, H., 2011. Novel detector design for reducing intercell x-ray cross-talk in the variable resolution x-ray CT scanner: a Monte Carlo study. Med. Phys. 38, 1389–1396.

Arabi, H., Asl, A.R.K., Ay, M.R., Zaidi, H., 2015. Monte Carlo-based assessment of the trade-off between spatial resolution, field-of-view and scattered radiation in the variable resolution X-ray CT scanner. Phys. Med. 31, 510–516.

Badea, C., Drangova, M., Holdsworth, D., Johnson, G., 2008. In vivo small-animal imaging using micro-CT and digital subtraction angiography. Phys. Med. Biol. 53, R319–R350.

Badea, C.T., Hedlund, L.W., Wheeler, C.T., Mai, W., Johnson, G.A., 2004. Volumetric microCT system for in vivo microscopy. In: Proceedings of the 2nd IEEE International Symposium on Biomedical Imaging: Nano to Macro, pp. 1377–1380.

Bartling, S.H., Stiller, W., Semmler, W., Kiessling, F., 2007. Small animal computed tomography imaging. Curr. Med. Imaging Rev. 3, 45–59.

Bretin, F., Warnock, G., Luxen, A., Plenevaux, A., Seret, A., Bahri, M.A., 2013. Performance evaluation and x-ray dose quantification for various scanning protocols of the GE eXplore 120 micro-CT. IEEE Trans. Nucl. Sci. 60, 3235–3241.

Bushberg, J.T., Boone, J.M., 2011. *The Essential Physics of Medical Imaging*. Lippincott Williams & Wilkins, Philadelphia, PA, USA.

Casali, F., Pasini, A., Romani, D., Talarico, F., 2003. Development of high resolution X-ray DR and CT systems for non-medical applications. In: Proceedings of the International Symposium on Computed Tomography and Image Processing for Industrial Radiology. Berlin, Germany, pp. 23–25.

De Clerck, N.M., Meurrens, K., Weiler, H., Van Dyck, D., Vanhoutte, G., Terpstra, P., Postnov, A.A., 2004. High-resolution X-ray microtomography for the detection of lung tumors in living mice. Neoplasia 6, 374–379.

Defrise, M., Clack, R., 1995. Filtered backprojection reconstruction of combined parallel beam and cone beam SPECT data. Phys. Med Biol. 40, 1517–1537.

Dobbins, J.T., Ergun, D.L., Rutz, L., Hinshaw, D.A., Blume, H., Clark, D.C., 1995. DQE (f) of four generations of computed radiography acquisition devices. Med. Phys. 22, 1581–1593.

Feldkamp, L., Davis, L., Kress, J., 1984. Practical cone-beam algorithm. JOSA A 1, 612–619.

Ford, N., Thornton, M., Holdsworth, D., 2003. Fundamental image quality limits for microcomputed tomography in small animals. Med. Phys. 30, 2869–2877.

Gupta, R., Cheung, A.C., Bartling, S.H., Lisauskas, J., Grasruck, M., Leidecker, C., Schmidt, B., Flohr, T., Brady, T.J., 2008. Flat-panel volume CT: fundamental principles, technology, and applications 1. Radiographics 28, 2009–2022.

Holdsworth, D.W., Thornton, M.M., 2002. Micro-CT in small animal and specimen imaging. Trends Biotechnol. 20, S34–S39.

Hu, Z., Gui, J., Zou, J., Rong, J., Zhang, Q., Zheng, H., Xia, D., 2011. Geometric calibration of a micro-CT system and performance for insect imaging. IEEE Trans. Inf. Technol. Biomed. 15, 655–660.

Hutchinson, J.C., Shelmerdine, S.C., Simcock, I.C., Sebire, N.J., Arthurs, O.J., 2017. Early clinical applications for imaging at microscopic detail: microfocus computed tomography (micro-CT). Br. J. Radiol. 90, 20170113.

Kamali-Asl, A., Arabi, H., Tamhidi, S., 2009. Optimization of magnification in a VRX CT scanner. In: Proceedings of the World Congress on Medical Physics and Biomedical Engineering September 7-12, 2009. Munich, Germany, Springer, pp. 266–269.

Khodadad, D., Ahmadian, A., Ay, M.R., Esfahani, A.F., Banaem, H.Y., Zaidi, H., 2011. B-spline based free form deformation thoracic non-rigid registration of CT and PET images. In: Proceedings of the International Conference on Graphic and Image Processing (ICGIP 2011), SPIE, 1-3 October 2011. Cairo, Egypt, pp. 82851K.

Laperre, K., Depypere, M., van Gastel, N., Torrekens, S., Moermans, K., Bogaerts, R., Maes, F., Carmeliet, G., 2011. Development of micro-CT protocols for in vivo follow-up of mouse bone architecture without major radiation side effects. Bone 49, 613–622.

Lin, C., Miller, J.D., 1996. Cone beam X-ray microtomography for three-dimensional liberation analysis in the 21st century. Int. J. Mineral. Process. 47, 61–73.

Melnyk, R., DiBianca, F.A., 2007. Modeling and measurement of the detector presampling MTF of a variable resolution x-ray CT scanner. Med. Phys. 34, 1062–1075.

Paulus, M.J., Gleason, S.S., Kennel, S.J., Hunsicker, P.R., Johnson, D.K., 2000. High resolution X-ray computed tomography: an emerging tool for small animal cancer research. Neoplasia 2, 62–70.

Ross, W., Cody, D.D., Hazle, J.D., 2006. Design and performance characteristics of a digital flat-panel computed tomography system. Med. Phys. 33, 1888–1901.

Samei, E., Ranger, N.T., Dobbins, J.T., Chen, Y., 2006. Intercomparison of methods for image quality characterization. I. Modulation transfer function. Med. Phys. 33, 1454–1465.

Seibert, J.A., 2006. Flat-panel detectors: how much better are they? Pediatr. Radiol. 36, 173.

Song, X., Frey, E., Tsui, B., 2001. Development and evaluation of a microCT system for small animal imaging. In: Proceedings of the IEEE Nuclear Science Symposium Conference Record, pp. 1600–1604.

Tuy, H.K., 1983. An inversion formula for cone-beam reconstruction. SIAM J. Appl. Math. 43, 546–552.

Vaquero, J.J., Redondo, S., Lage, E., Abella, M., Sisniega, A., Tapias, G., Montenegro, M.L.S., Desco, M., 2008. Assessment of a new high-performance small-animal X-ray tomograph. IEEE Trans. Nucl. Sci. 55, 898–905.

Zainon, R., Butler, A., Cook, N., Butzer, J., Schleich, N., De Ruiter, N., Tlustos, L., Clark, M.J., Heinz, R., Butler, P.H., 2010. Construction and operation of the MARS-CT scanner. Internetw. Indones. J. 2, 3–10.

Zhu, S., Tian, J., Yan, G., Qin, C., Feng, J., 2009a. Cone beam micro-CT system for small animal imaging and performance evaluation. J. Biomed. Imaging 2009, 16.

Zhu, S., Tian, J., Yan, G., Qin, C., Liu, J., 2009b. An experimental cone-beam micro-CT system for small animal imaging. In: Proceedings of the SPIE Medical Imaging. International Society for Optics and Photonics, pp. 72582S-72582S-72510.